Absence of zero-energy surface bound states in Cu_{x}Bi_{2}Se_{3} studied via Andreev reflection spectroscopy

Haibing Peng, Debtanu De, Bing Lv, Fengyan Wei, and Ching-Wu Chu

Phys. Rev. B **88**, 024515 — Published 25 July 2013

DOI: 10.1103/PhysRevB.88.024515

Absence of zero-energy surface bound states in $Cu_xBi_2Se_3$ via a study of Andreev reflection spectroscopy

Haibing Peng *, Debtanu De, Bing Lv, Fengyan Wei, Ching-Wu Chu †

Department of Physics and the Texas Center for Superconductivity, University of Houston, Houston, Texas 77204-5005, USA

* haibingpeng@uh.edu

† cwchu@uh.edu

ABSTRACT

$Cu_xBi_2Se_3$ has been proposed as a potential topological superconductor characterized by an odd-parity full bulk superconducting gap and zero-energy surface Andreev bound states (Majorana fermions). A predicted consequence of such Majorana fermions is a peak in the zero-energy density of states which should lead to a persistent zero-bias-conductance-peak (ZBCP) in Andreev reflection (AR) or tunneling experiments. Here we employ a newly developed nanoscale AR spectroscopy method to study normal metal/superconductor (N-S) devices featuring $Cu_xBi_2Se_3$. The results show that a ZBCP can be tuned in or out from $Cu_xBi_2Se_3$ samples depending on the N-S barrier strength. While the appearance of ZBCP may be traced to different origins, its absence under finite barrier strength represents the absence of zero-energy Majorana fermions. The present observations thus call for a reexamination of the intriguing superconductivity in $Cu_xBi_2Se_3$.

I. Introduction

Novel quantum states of matter with topological characteristics have been emerging as exciting research topics since the discovery of topological insulators.[1-5] Protected by time-reversal symmetry, a topological insulator (e.g., Bi_2Se_3) [6, 7] possesses a full band gap in the bulk, but has gapless surface states with an odd number of Dirac points. In analogy, with particle-hole symmetry considered, topological superconductors [8-14] were theoretically predicted to exist with a full bulk superconducting (SC) gap but stable gapless surface bound states (Majorana fermions). Under active research is the experimental search for topological superconductors and initial potential candidates include the ^{3}He-B phase [8, 9]and the interface between a topological insulator and an s-wave superconductor.[10] Particularly, the recent discovery of superconductivity in the electron-doped topological insulator $Cu_xBi_2Se_3$ [15] has generated great interest and immediately drew attention [16, 17] on its implication for the search of Majorana fermions and topological superconductors. It has been proposed that an odd parity pairing could be induced due to strong spin-orbital coupling in $Cu_xBi_2Se_3$, which should then meet the criteria for a topological superconductor.[16] In this model, two-orbital effective short-range electron interactions are assumed to be responsible for the superconductivity and as a result a topological superconductor phase occurs for certain range of interaction strength. Majorana fermions then manifest themselves in a Kramers pair of zero-energy surface Andreev bound states. Therefore, a central idea for experimentally identifying the topological superconductor phase is to detect a peak of density of states at zero energy (as predicted for the Majorana fermions).[18] Recently, a zero-bias-conductance-peak (ZBCP) was observed in Andreev reflection (AR) spectra for normal metal/superconductor (N-S) junctions made by a soft point-contact method,[18] and this result was interpreted as the evidence for topological

superconductivity in $Cu_xBi_2Se_3$. However, if there does exist a peak in the zero-energy density of states (as a result of the existence of Majorana fermions), the ZBCP should occur persistently in all N-S junctions with different barrier strength Z ranging from the transparent limit to the tunneling limit. Therefore, further stringent experimental test is called for to confirm the existence of Majorana fermions in $Cu_xBi_2Se_3$. Here we have employed a unique nano-scale AR spectroscopy method [19] to construct N-S junctions featuring $Cu_xBi_2Se_3$ with different barrier strength Z and elucidate the SC gap structures of $Cu_xBi_2Se_3$ as a function of temperature and magnetic field. Our results show that the ZBCP can be tuned in or out from $Cu_xBi_2Se_3$ samples depending on the N-S barrier strength Z. While the appearance of ZBCP may be traced to different origins, its absence under finite barrier strength represents the absence of a zero-energy density-of-states peak. The present observations thus call for a reexamination of the nature of the superconducting state in $Cu_xBi_2Se_3$, presumably the representative (if not the only) topological superconductor discovered to date.

II. Experiment

We used a newly developed technique [19] to construct nanoscale N-S devices and perform AR spectroscopy. In brief, we mechanically cleaved the bulk material of $Cu_xBi_2Se_3$ with Tc ~3.4 K [20] into micro-scale crystals, immediately transferred them into a vacuum chamber (~ 10^{-5} Torr), and used a sharp probe tip attached on a micro-manipulator to place a piece of microcrystal on top of multiple parallel metal electrodes spaced ~ 500 nm apart as designed via electron-beam lithography (Fig. 1a). To obtain AR spectra for a target N-S junction, we used a special circuit [19] (Fig. 1b) where a small AC current superimposed to a DC bias current is applied between the I_+ and I_- terminals while both the DC and the AC voltages across the N-S junction are measured between the V_+ and V_- terminals. Therefore, the AR

spectrum, i.e. the differential conductance *dI/dV* vs. the DC voltage *V* across the target junction between the I_+ (V_+) terminal and the superconductor, is obtained. The flexibility in selecting the configuration for measurement terminals allows the study of multiple N-S junctions between different metal electrodes and the same superconductor crystal with different *Z* parameters in a single device.

III. Result and discussion

Figs. 1c-1e show the normalized *dI/dV* vs. *V* at *T* = 240 mK for three N-S junctions. The AR spectra (symbols) demonstrate a *dI/dV* dip at zero bias and two shoulders at $V \sim \pm 0.4$ mV, which is typical for N-S interface with finite barrier strength *Z* according to the BTK theory.[21] The solid lines are fittings of the experimental data by the generalized BTK theory.[22, 23] Considering the coexistence of superconducting and non-superconducting phases in bulk $Cu_xBi_2Se_3$, [15] we can express the total normalized conductance as $\sigma = w\sigma_s + (1-w)$, where σ_s is the normalized conductance for the interface between the normal metal and the superconducting phase, calculated according to the BTK theory,[22] and *w* is the weight of contribution to conductance from the superconducting phase in the nano-scale junction (*w* is related to the superconducting volume fraction). For the expression of σ_s, we use the formula for a single isotropic s-wave superconducting gap in the zero-temperature limit [Ref. 22]:

$$\sigma_s = \frac{1 + A(E) - B(E)}{\tau_N},$$

where $E = eV$, $\tau_N = \frac{1}{1+Z^2}$, $A(E) = \frac{\sqrt{(\alpha^2+\eta^2)(\beta^2+\eta^2)}}{\gamma^2}$,

$$B(E) = Z^2 \frac{\{Z(\alpha-\beta)-2\eta\}^2 + \{(\alpha-\beta)+2Z\eta\}^2}{\gamma^2},$$

$\gamma^2 \equiv \{\alpha + Z^2(\alpha - \beta)\}^2 + \{\eta(2Z^2+1)\}^2$, $\alpha \equiv \mathrm{Re}[u_0{}^2]$, $\beta \equiv 1-\alpha$, $\eta \equiv \mathrm{Im}[u_0{}^2]$, and

$u_0{}^2 \equiv \frac{1}{2}\left[1 + \frac{\sqrt{(E+i\Gamma)^2 - \Delta^2}}{(E+i\Gamma)}\right]$. Note that σ_s is completely determined by three fitting parameters: the SC gap value Δ, the broadening parameter Γ and the barrier strength *Z*.

From the fitting of these AR spectra in Fig. 1, we obtain the SC gap energy as Δ = 0.35 ± 0.04 meV (with the broadening parameter Γ ranging from 0.13 to 0.27 meV). The weight of contribution varies significantly from *w* = 13% to 80%, which indicates electronic phase separation on microscopic scale and is consistent with the low superconducting volume fraction (up to ~ 20%) for the bulk material.[20] Notably, despite of different barrier strength and junction characteristics, all three N-S junctions from different samples reproducibly give similar values of gap energy Δ ~ 0.35 meV, demonstrating that spectroscopic, energy-resolved information of the SC gap is achieved. We note that those spectroscopic N-S junctions (Fig. 1) usually show a large normal state resistance R_N (> 100 Ω), but for junctions with R_N smaller than 10 Ω (Fig. 2) the energy scale is not accurate and we usually observe a ZBCP. This observation is consistent with an empirical rule [24] for determining ballistic transport regime: $R_N >> 4\rho/3\pi l$, with *l* the mean free path of electrons in the junction and *ρ* the bulk material resistivity, since ballistic transport across the N-S interface is sufficient for providing spectroscopic, energy-resolved information of the SC gap (see Ref. [20] for more discussions). By using bulk *ρ* ~ 140 μΩcm and *l* ~ 45 nm,[25] we find that $R_N >> 13$ Ω can be used as the criteria for selecting ballistic N-S junctions in $Cu_xBi_2Se_3$.

In contrast, the junctions with smaller R_N (Fig. 2) display a conductance peak at zero bias, which is typical for nearly transparent N-S interface with weak barrier strength. The ZBCP can in principle have various sources of origin, such as the conductance enhancement (plateau)

due to Andreev reflection resulting from bulk SC gaps, or a zero-energy density-of-states peak due to potential surface Andreev bound states.[18] However, the absence of a ZBCP in the junctions with finite barrier strength (Fig. 1) indicates that the ZBCP observed in $Cu_xBi_2Se_3$ is unlikely due to the existence of zero-energy surface Andreev bound states. Instead, the ZBCP can be consistently explained as the Andreev reflection plateau due to the bulk SC gap but with a cut-off of plateau width when the critical current is reached at relatively low bias $V < \Delta/e$ because of the low junction resistance.[19] For the junctions of Figs. 2b and 2c, the width of the ZBCP does not give the gap energy correctly, because the normal-state resistance R_N is less than the aforementioned threshold R_N value for ballisticity (~ 13 Ω) and thus these junctions are in a transport regime dominated by energy-changing inelastic scattering. On the other hand, for the junction of Fig. 2a, R_N is close to the threshold value ~ 13 Ω, and thus the peak width is similar to the energy gap ~ 0.35 meV as obtained from Fig. 1. To better elucidate the nature of the ZBCP, we performed measurements again after a period of six months for the low-conductance junctions of Figs. 2b and 2c. The new results (see Fig. S3 of Ref. [20]) show that their normal-state resistance R_N is increased to ~ 100 Ω (an order of magnitude higher than the initial values in Figs. 2b and 2c) and the extracted gap values are now similar to those from the junctions of Fig. 1, which is consistent with our previous discussion on the determination of spectroscopic conditions based on R_N values and confirms that the observed ZBCP should be a consequence of the bulk SC gap.

In Fig. 3, we present the AR spectra as a function of both magnetic field and temperature for one N-S junction with large R_N (finite barrier strength) and another with smaller R_N (transparent barrier).[20] For the junction with finite barrier strength (Fig. 3a), as magnetic field increases, the double peaks (characterizing the SC gap) in the AR spectrum become less and less

pronounced up to B = 3T and completely disappear at B = 5 T (close to the upper critical-field B_{c2} reported for bulk $Cu_xBi_2Se_3$ [25]). The dips at high bias move towards the center in a pace much faster than that for the gap-related double peaks, and the dip position reflects a decreasing critical current as the B field (or temperature) increases since the dips characterize the breaking of superconducting state at the critical current.[19] As temperature increases (Fig. 3b), the SC gap (double peaks) shrinks slowly up to T = 1.1 K. At T = 1.5 K, the AR spectrum changes into a single broad bump (as often observed for other finite-barrier junctions [20]), which can be understood within the BTK theory as the reduction of barrier strength *Z* due to thermally activated transport across the interface. The *dI/dV* spectrum becomes V-shaped above T = 2 K but continues to evolve even at T = 4.3 K (above bulk Tc).

For the junction with transparent barrier (Fig. 3c), the ZBCP is greatly suppressed at B = 3 T and disappears at B = 5 T. As a function of temperature (Fig. 3d), a broad bump persists above bulk Tc and disappears at T ~ 4.5 K. Notable features besides the ZBCP are the *dI/dV* oscillations at high bias before reaching the normal state. The positions of such oscillations shift towards lower bias as T increases, until they disappear at T = 4K. As discussed before, the broad dip outside of the SC gap can be attributed to the role of the critical current,[19] yet the origin of the *dI/dV* oscillations within the broad dip is not clear. Nevertheless, the overall evolution of the AR spectra as a function of magnetic field and temperature can be consistently interpreted as a result for a single-gap bulk superconductor.[21, 26-27]

In Ref. [18], a zero-energy density-of-states peak due to Majorana fermions was invoked to explain a ZBCP observed therein. However, we note in particular that the representative AR spectra in Ref. [18] show a ZBCP on top of a strong non-saturating V-shape background in the *dI/dV vs. V* curve, and the ZBCP observed therein disappears completely in a magnetic field ~

0.45 T (an order of magnitude smaller than the upper critical field reported for bulk $Cu_xBi_2Se_3$ [25]). To address this issue, we performed control experiments to produce N-S junctions showing either a ZBCP with a strong non-saturating V-shape background (Figs. 4a - 4c) or a pure V-shape *dI/dV* spectrum without ZBCP (Figs. 4d – 4f). It is important to stress that these two N-S junctions of Fig. 4 were not electrically connected initially after placing a superconductor microcrystal on top of parallel metal electrodes, but electrical connection was later established by applying a short voltage pulse (~ 10 V in magnitude) to anneal the contacts. Notably, both junctions (connected after voltage annealing) show a common strong non-saturating V-shape background. For one annealed junction (Figs. 4a-4c), a ZBCP is observed but disappears at a magnetic field only ~ 0.4T (Fig. 4b), indicating a thick degraded superconducting surface layer dominating the N-S transport. The other annealed junction (Figs. 4d - 4f) shows a pure strong V-shape spectrum with no hint for Andreev reflection, pointing towards a thick non-superconducting surface layer (we also note that the V-shape background for both junctions of Fig. 4 shows similar temperature and B-field dependence, which cautions any interpretation by the "pseudo-gap" behavior above Tc [18]). In stark contrast, for two additional junctions in the same device of Fig. 4 which were electrically connected initially without the need of voltage annealing (see Fig. S5 in Ref. [20]), the AR spectra are dominated by a pronounced ZBCP but with much smaller V-shape background (indicating less contribution from a non-superconducting surface layer), and the ZBCP is suppressed at higher B-field ~ 2 T (indicating better-quality superconductor layers at the junctions). Therefore, our control experiments caution that a ZBCP disappearing at magnetic fields much lower than the bulk critical field and showing a strong non-saturating V-shape background reflects the existence of a

degraded superconducting surface layer in non-ideal N-S junctions, and thus cannot be used as the signature for zero-energy Majorana fermions.

IV. Conclusion

In summary, the experiments can be consistently explained by bulk-gap Andreev reflection in combination with the effect of critical current. For the same piece of superconductor microcrystal, a zero-bias conductance peak occurs for N-S junctions with transparent barriers (see Fig. 2), but is absent in N-S junctions with finite barriers showing archetypical double-peak AR spectra (see Fig. 1), which rules out the existence of zero-energy surface bound states in $Cu_xBi_2Se_3$. The overall evolution of the AR spectra as a function of magnetic field and temperature can be well described by the result from a single-gap bulk superconductor. Therefore, the zero-bias conductance peak observed in $Cu_xBi_2Se_3$ does not represent an evidence for the existence of characteristic zero-energy Majorana fermions for topological superconductors. Note: recently, an independent study by tunneling experiments also shows that there is no peak of density of states within the bulk superconducting gap. [28]

Acknowledgements

This work was supported by the NSF Award No. ECCS-1247874 under the program director Dr. Anupama Kaul.

Appendix

A.1. Growth and characterization of bulk crystals of $Cu_xBi_2Se_3$

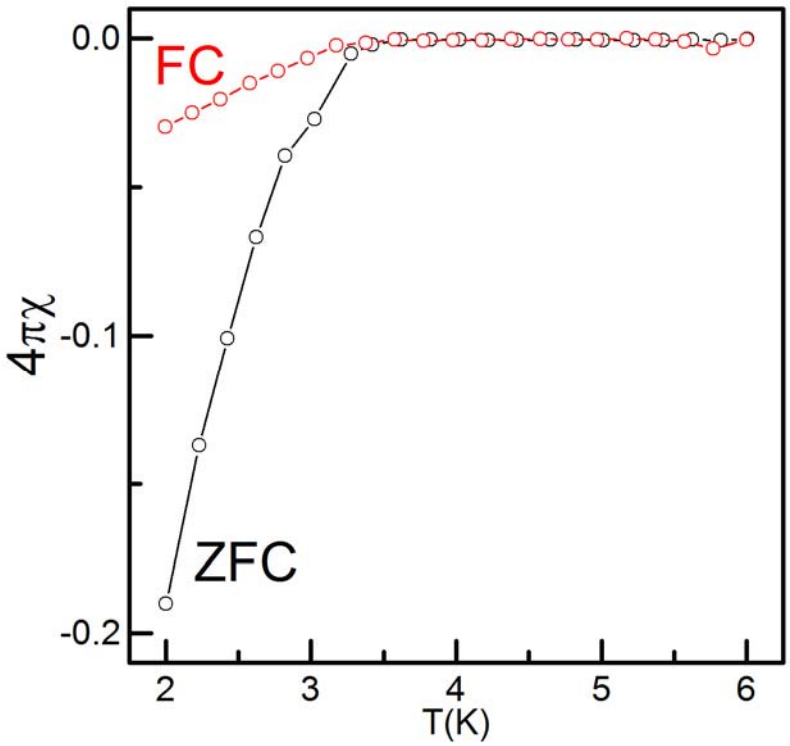

Fig. S1. Magnetic susceptibility as a function of temperature for the bulk material of $Cu_xBi_2Se_3$.

We started with single-crystal bulk materials of $Cu_xBi_2Se_3$ with $x \sim 0.15$, synthesized using a method similar to previous reports. [Ref. 15] Single crystals of $Cu_xBi_2Se_3$ up to cm size with c-axis preferred orientation are grown by slowly cooling of the melting mixture. The reactant mixture of Bi(99.999% pure), Cu (99.995% pure), and Se (99.999% pure), is sealed in a quartz tube under vacuum, heated up to 860 ^oC for 20 hrs, slowly cooled down to 600 ^oC over 3 days, and then quenched in cold water. X-ray diffraction pattern in θ-2θ scan confirms the single crystallinity of the samples and measured rocking curves show a full width at half maximum of 0.3 degree for the (0 0 15) peak. Magnetic susceptibility measurement (Fig. S1) indicates an on-

set bulk Tc ~3.4 K and a superconducting volume fraction up to ~ 20 % at 2 K, close to results previously reported. [Ref. 15]

A.2. A discussion on the determination of transport regimes in a N-S junction to obtain spectroscopic (i.e. energy-resolved) information

In principle, the superconducting gap energy can only be measured accurately in either the ballistic transport regime with the actual N-S point contact radius a much less than the electron mean free path l, or in the diffusive regime with no significant inelastic scattering (albeit introducing a non-ideal effect of reducing the Andreev refection ratio). In the so-called thermal regime with significant inelastic scattering, the Andreev reflection spectrum can be distorted by energy-changing scattering events and the gap energy may not be obtained accurately from the experimental data. For ballistic conduction through a restriction (e.g., a typical point contact with a radius a), the electrical resistance at the normal state can be expressed by the Sharvin formula as $R_N = (4\rho l)/(3\pi a^2)$, with ρ the bulk material resistivity of the normal state for the superconductor. In the case of only one point contact dominating the conduction in a real N-S junction, the ballistic condition $a << l$ can then be turned into a condition on the normal-state contact resistance: $R_N >> 4\rho/3\pi l$. This has been commonly used as an empirical criterion for determining ballisticity, since the normal-state resistance R_N can be measured in experiments (but the radius of a real point contact is experimentally inaccessible in general). More information on the use of the normal-state resistance to estimate the point-contact size and thus determine the ballisticity of a junction can be found in review papers on this topic, e.g., pages 3158-3159 in *J. Phys.: Condens. Matter* **1,** 3157 (1989) (by Duif et al.); page 8 in

arXiv:physics/0312016v1 (by Naidyuk and Yanson); and pages 2-4 in S*upercond. Sci. & Tech.* **23,** 043001 (2010) (by Daghero and Gonnelli).

In the case of multiple parallel point contacts contributing to the conduction in a N-S junction, the normal-state resistance of each individual contact is larger than the measured total normal-state resistance R_N (i.e. the resistance of the whole N-S junction). Therefore, as long as the measured normal-state resistance $R_N >> 4\rho/3\pi l$, the N-S junction (either with single or multiple contacts) showing Andreev reflection should be ballistic.

A.3. Supplementary figures (Fig. S2 – S5)

Below we present more data (Fig. S2) for the N-S junction of Fig. 1e, the AR spectra measured again (Fig. S3) after 6 months for the junctions of Figs. 2b and 2c, the normalized AR spectra (Fig. S4) for the junctions of Fig. 3, and the AR spectra (Fig. S5) of two other junctions for the device of Fig. 4.

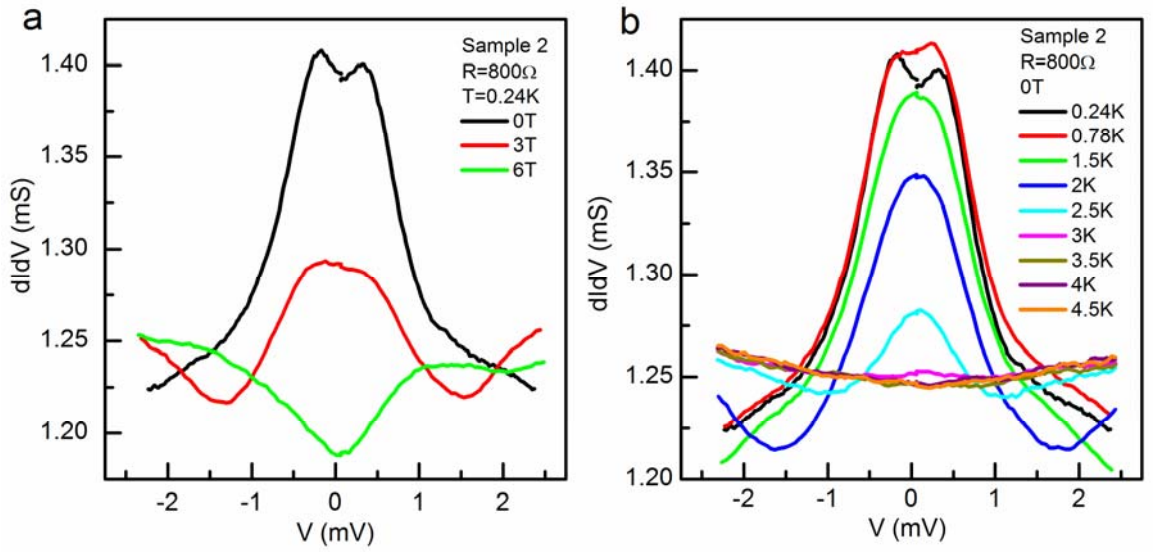

Fig. S2. *dI*/*dV* vs. *V* measured (a) under different magnetic fields perpendicular to the substrate at $T = 240$ mK and (b) at different temperatures with $B = 0$ for the N-S junction shown in Fig. 1e of the main text.

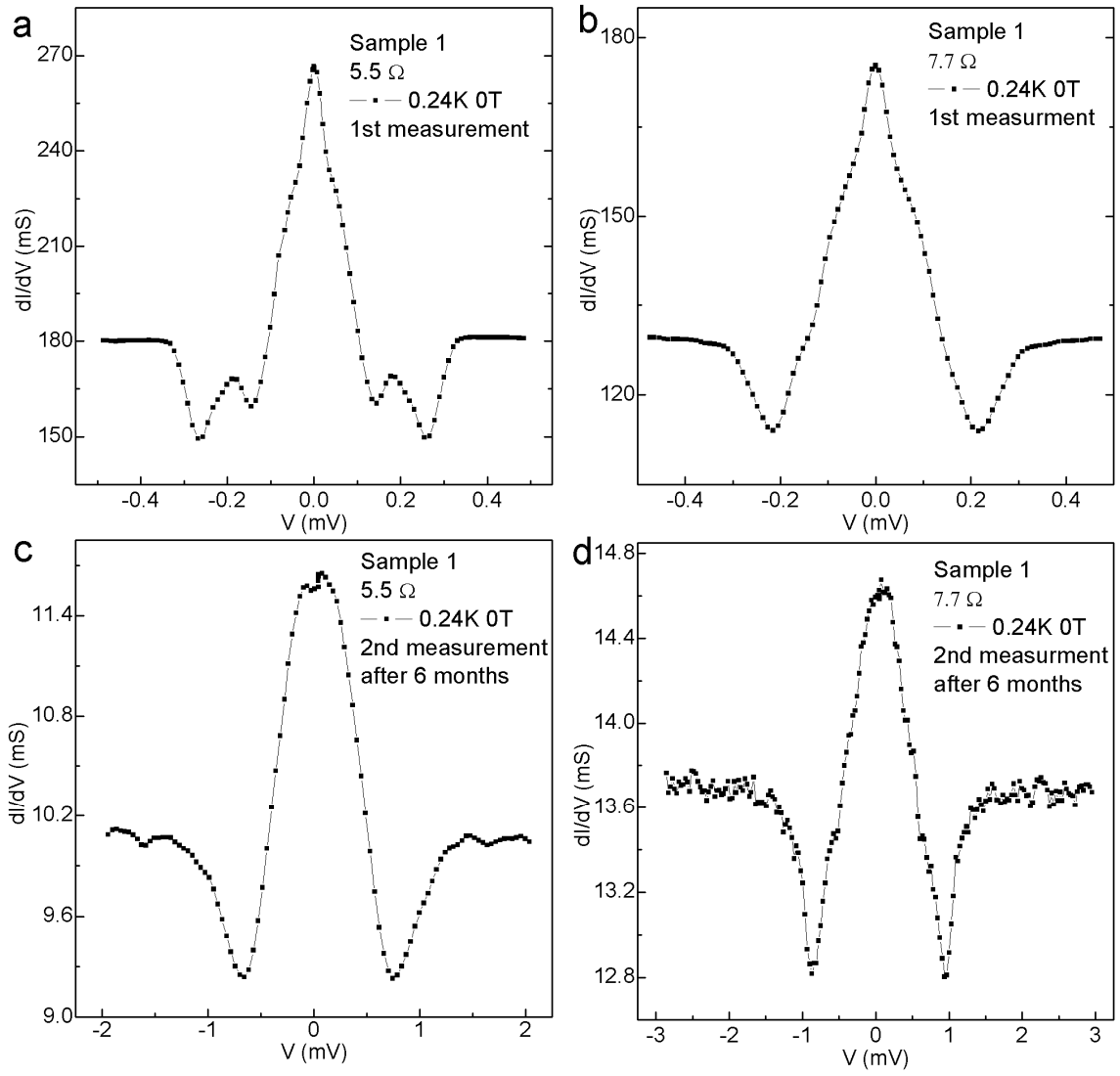

Fig. S3 Comparison between AR spectra in the first measurement (top, replots of Figs. 2b and 2c in the main text) and in the second measurement after a period of six months for the same junctions shown in Figs. 2b and 2c of the main text. The device was preserved in a desiccator during the period between the measurements. The image of the device is shown in Fig. 1a of the main text. In the second measurement, only three electrodes (labeled as #1, #2, and #6 in Fig.

1a) are still electrically connected to the superconductor crystal, which are usable for implementing the measurement by the circuit of Fig. 1b in the main text. The junction shown in the left (right) column is at electrode #1 (#6).

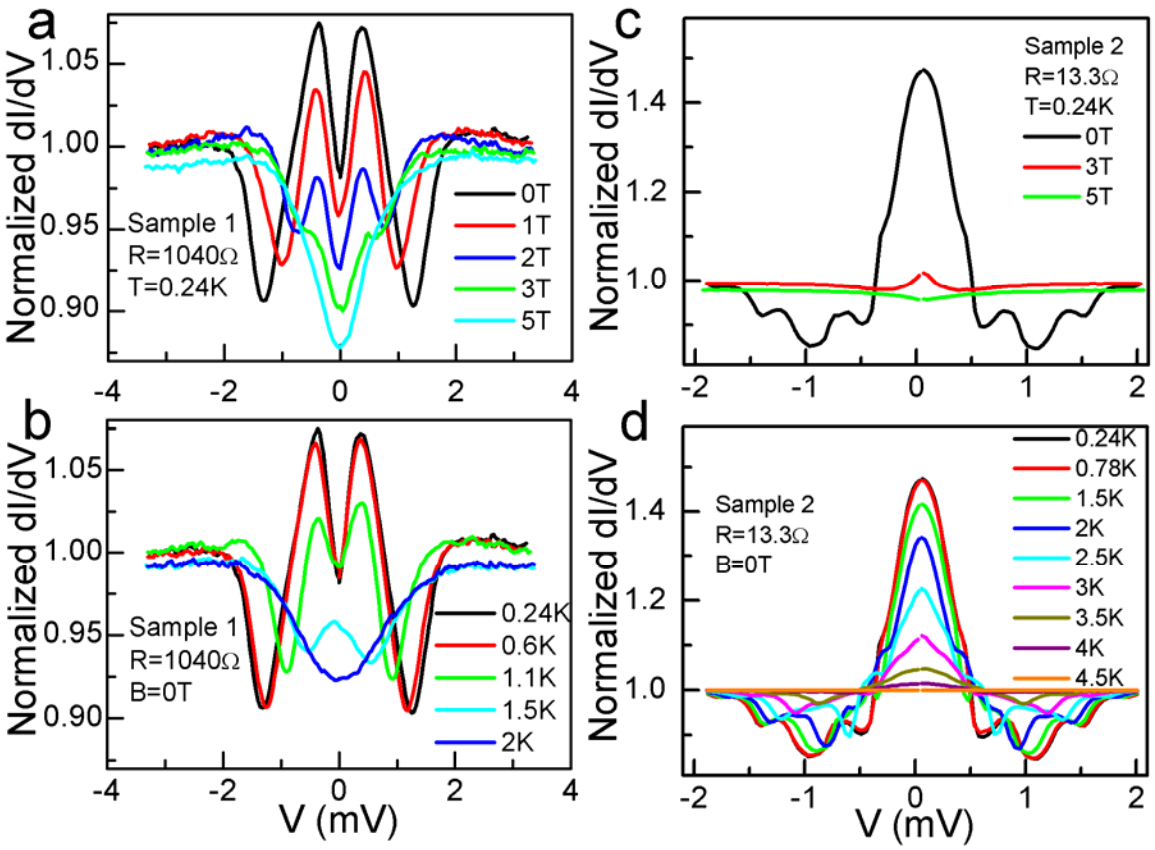

Fig. S4 The normalized dI/dV data for the junctions shown in Fig. 3 of the main text. For (a) and (b), the raw dI/dV data are divided by adjusted normal-state data which are obtained by offset the raw dI/dV spectrum at T = 4.3 K to match the high-bias dI/dV spectrum at T = 240 mK. For (c) and (d), the raw dI/dV data are divided directly by the raw dI/dV spectrum at T = 4.5 K.

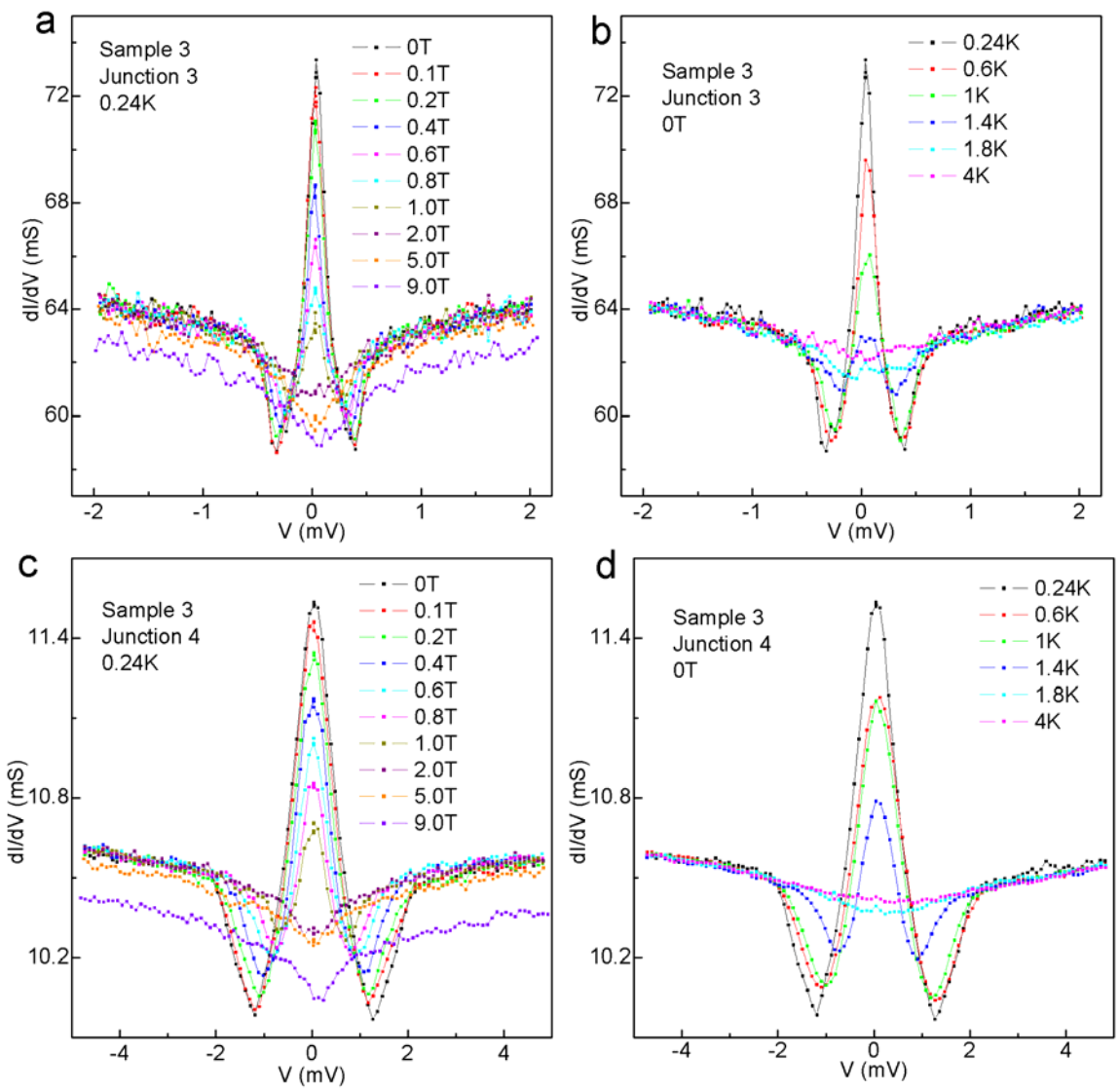

Fig. S5 *dI*/*dV* vs. *V* measured under different magnetic fields perpendicular to the substrate at *T* = 240 mK (left column) and at different temperatures with *B* = 0 (right column) for other two junctions in the same device of Fig. 4 in the main text. These two junctions were electrically connected initially without the need of voltage annealing, and they are located at the two outermost electrodes (i.e., #1 and #6) similar to the pattern shown in Fig. 1a of the main text. With four electrically connected junctions in this device, we also obtained the four-terminal resistance of the superconductor microcrystal to be 0.2 Ω above T_c (typical for other devices), which is negligible compared with the junction normal-state resistance R_N.

References

[1] C. L. Kane, and E. J. Mele, Phys. Rev. Lett. **95**, 146802 (2005).
[2] B. A. Bernevig, T. L. Hughes, and S. C. Zhang, Science **314**, 1757 (2006).
[3] B. A. Bernevig, and S. C. Zhang, Phys. Rev. Lett. **96**, 106802 (2006).
[4] C. L. Kane, and E. J. Mele, Phys. Rev. Lett. **95**, 226801 (2005).
[5] M. Konig, S. Wiedmann, C. Brune, A. Roth, H. Buhmann, L. W. Molenkamp, X. L. Qi, and S. C. Zhang, Science **318**, 766 (2007).
[6] H. J. Zhang, C. X. Liu, X. L. Qi, X. Dai, Z. Fang, and S. C. Zhang, Nat. Phys. **5**, 438 (2009).
[7] Y. Xia *et al.*, Nat. Phys. **5**, 398 (2009).
[8] A. P. Schnyder, S. Ryu, A. Furusaki, and A. W. W. Ludwig, Phys. Rev. B **78**, 195125 (2008).
[9] R. Roy, arXiv:0803.2868v1 (2008).
[10] L. Fu, and C. L. Kane, Phys. Rev. Lett. **100**, 096407 (2008).
[11] X. L. Qi, T. L. Hughes, S. Raghu, and S. C. Zhang, Phys. Rev. Lett. **102**, 187001 (2009).
[12] A. Kitaev, in *Advances in Theoretical Physics*2009), p. 22.
[13] X. L. Qi, T. L. Hughes, and S. C. Zhang, Phys. Rev. B **81**, 134508 (2010).
[14] M. Sato, Phys. Rev. B **81**, 220504 (2010).
[15] Y. S. Hor *et al.*, Phys. Rev. Lett. **104**, 057001 (2010).
[16] L. A. Fu, and E. Berg, Phys. Rev. Lett. **105**, 097001 (2010).
[17] L. A. Wray *et al.*, Nat. Phys. **6**, 855 (2010).
[18] S. Sasaki, M. Kriener, K. Segawa, K. Yada, Y. Tanaka, M. Sato, and Y. Ando, Phys. Rev. Lett. **107**, 217001 (2011).
[19] H. B. Peng, D. De, Z. Wu, and C. Diaz-pinto, Journal of Physics: Condensed Matter **24**, 455703 (2012).
[20] See Appendix for bulk-material information (Fig. S1), a discussion of spectroscopic transport regimes, more data (Fig. S2) for the N-S junction of Fig. 1e, the AR spectra measured again (Fig. S3) after 6 months for the junctions of Figs. 2b and 2c, the normalized AR spectra (Fig. S4) for the junctions of Fig. 3, and the AR spectra (Fig. S5) of two other junctions for the device of Fig. 4.
[21] G. E. Blonder, M. Tinkham, and T. M. Klapwijk, Phys. Rev. B **25**, 4515 (1982).
[22] A. Plecenik, M. Grajcar, S. Benacka, P. Seidel, and A. Pfuch, Phys. Rev. B **49**, 10016 (1994).
[23] R. C. Dynes, V. Narayanamurti, and J. P. Garno, Phys. Rev. Lett. **41**, 1509 (1978).
[24] D. Daghero, and R. S. Gonnelli, Superconductor Science & Technology **23**, 043001 (2010).
[25] T. V. Bay, T. Naka, Y. K. Huang, H. Luigjes, M. S. Golden, and A. de Visser, Phys. Rev. Lett. **108**, 057001 (2012).
[26] G. Deutscher, Reviews of Modern Physics **77**, 109 (2005).
[27] We have noticed that both ZBCP and double conductance peaks (at finite bias) were predicted recently for different types of Majorana fermions [A. Yamakage, K. Yada, M. Sato, Y. Tanaka, Phys. Rev. B 85, 180509 (2012)]. However, this has to be justified in the case of CuxBi2Se3, and particularly the contribution of the bulk SC gap has to be considered.
[28] Levy et al., arXiv:1211.0267 (2012).

Figure Captions

Figure 1. (a) Optical microscope image of a device with a $Cu_xBi_2Se_3$ microcrystal lying on six parallel metal electrodes (35 nm Pd/ 5 nm Cr) on a SiO_2/Si substrate. The four center electrodes (labeled as 2-5) are 1 μm wide while the two outside electrodes (labeled as 1 and 6) are 4 μm wide. For this sample, four metal electrodes are electrically connected to the superconductor microcrystal and the corresponding data are shown in Figs. 1 and 2. (b) Schematic diagram of a superconductor microcrystal on top of three normal metal electrodes and a circuit for obtaining Andreev reflection spectra for the target N-S junction between the I_+ (V_+) electrode and the superconductor. (c-e) Normalized differential conductance dI/dV (symbols) versus bias voltage V at temperature T = 240 mK and magnetic field B = 0 for three N-S junctions and the fitting to the data (solid lines) by the BTK theory (see main text). The fitting parameters are: (c) Δ = 0.32 meV, Γ = 0.21 meV, w = 61%, and Z = 0.7; (d) Δ = 0.35 meV, Γ = 0.13 meV, w = 13%, and Z = 0.45; (e) Δ = 0.39 meV, Γ = 0.27 meV, w = 80%, and Z = 0.38. The data of (c) and (d) are from the N-S junctions at electrode # 2 and #3, respectively, for the sample shown in Fig. 1a, and the data of (e) is from a different sample. The normalized dI/dV is obtained by dividing the measured dI/dV data at T =240 mK by appropriate normal-state data at T above bulk T_c. For the data of (e), the normal state is not reached within the measured bias-voltage range, but can be determined from the temperature dependence of AR spectra (see Fig. S2 of Ref. [20]).

Figure 2. dI/dV vs. V at T = 240 mK and B = 0 for three N-S junctions with smaller normal state resistance R_N. The junction of (a) is from the same sample as the junction of Fig. 1e, and the junctions of (b) and (c) are at electrode #1 and #6, respectively, for the sample of Fig. 1a.

Figure 3. dI/dV vs. V measured under different magnetic fields perpendicular to the substrate at T = 240 mK (top) and at different temperatures with B = 0 (bottom): (a)&(b) for the N-S junction of Fig. 1c, and (c) & (d) for the junction of Fig. 2a.

Figure 4. dI/dV vs. V measured at T = 240 mK and B = 0 (top); under different magnetic fields perpendicular to the substrate at T = 240 mK (center); and at different temperatures with B = 0 (bottom) for two N-S junctions of the same superconductor microcrystal in a device. These two N-S junctions were not electrically connected initially, but electrical connection was established after a short voltage pulse (~ 10 V in magnitude) was applied to anneal the contacts.

Figures

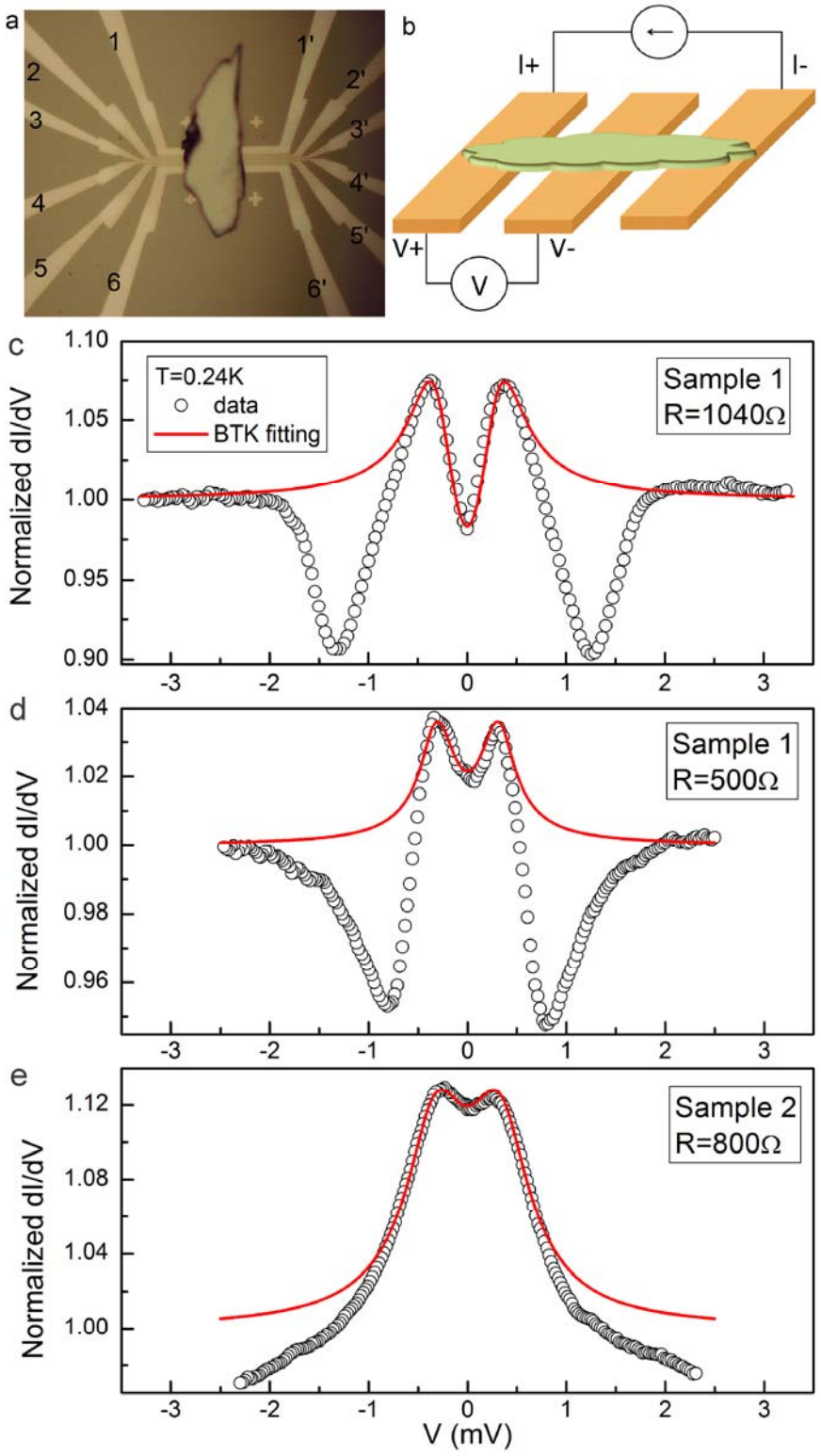

Fig. 1

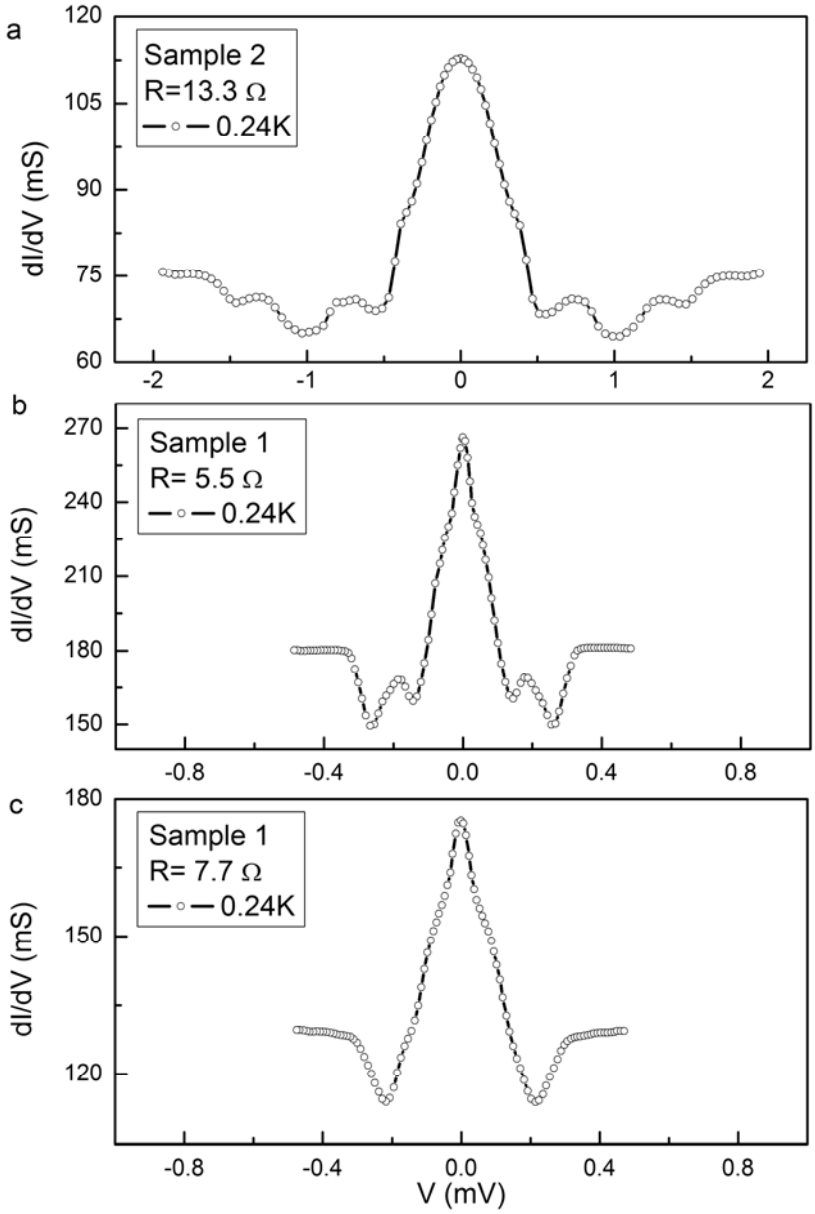
a
Sample 2
R=13.3 Ω
0.24K
dI/dV (mS)
120
105
90
75
60
-2
-1
0
1
2
b
Sample 1
R= 5.5 Ω
0.24K
dI/dV (mS)
270
240
210
180
150
-0.8
-0.4
0.0
0.4
0.8
c
Sample 1
R= 7.7 Ω
0.24K
dI/dV (mS)
180
150
120
-0.8
-0.4
0.0
0.4
0.8
V (mV)

Fig. 2

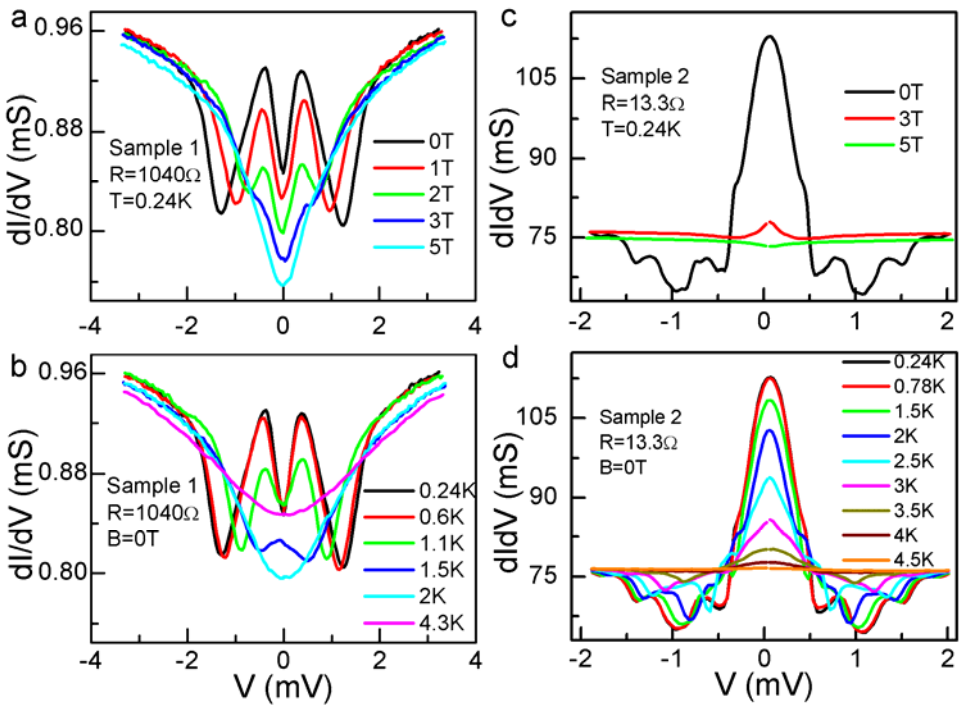
a
0.96
0.88
0.80
dI/dV (mS)
Sample 1
R=1040Ω
T=0.24K
0T
1T
2T
3T
5T
-4
-2
0
2
4
b
0.96
0.88
0.80
dI/dV (mS)
Sample 1
R=1040Ω
B=0T
0.24K
0.6K
1.1K
1.5K
2K
4.3K
V (mV)
c
105
90
75
dIdV (mS)
Sample 2
R=13.3Ω
T=0.24K
0T
3T
5T
-2
-1
0
1
2
d
105
90
75
dIdV (mS)
Sample 2
R=13.3Ω
B=0T
0.24K
0.78K
1.5K
2K
2.5K
3K
3.5K
4K
4.5K
V (mV)

Fig. 3

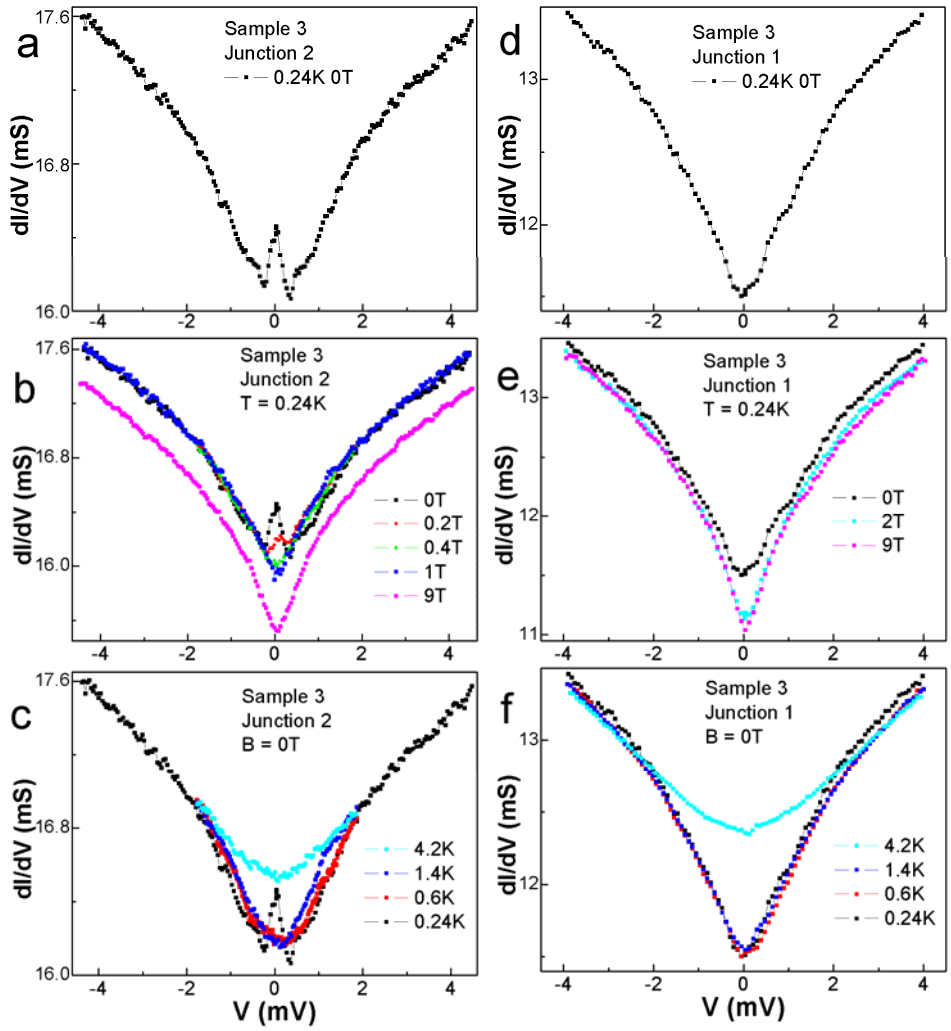
a
Sample 3
Junction 2
0.24K 0T
dI/dV (mS)
b
Sample 3
Junction 2
T = 0.24K
0T
0.2T
0.4T
1T
9T
c
Sample 3
Junction 2
B = 0T
4.2K
1.4K
0.6K
0.24K
V (mV)
d
Sample 3
Junction 1
0.24K 0T
e
Sample 3
Junction 1
T = 0.24K
0T
2T
9T
f
Sample 3
Junction 1
B = 0T
4.2K
1.4K
0.6K
0.24K
V (mV)

Fig. 4